Inorganic Chemistry
Article
pubs.acs.org/IC

First-Principles Study on Doping Effects of Sodium in Kesterite Cu_2ZnSnS_4

Zong-Yan Zhao* and Xiang Zhao

Faculty of Materials Science and Engineering, Key Laboratory of Advanced Materials of Yunnan Province, Kunming University of Science and Technology, 253# Xuefu Road, Kunming 650093, People's Republic of China

ABSTRACT: A sodium impurity is inevitable for Cu_2ZnSnS_4 on a substrate of soda−lime glass during high-temperature processing. Recently, it was found that a sodium impurity could improve the photovoltaic properties of Cu_2ZnSnS_4-based thin film solar cells (including influencing crystallinity, affecting grain growth, increasing hole density, shifting the acceptor level closer to the conduction band, increasing carrier concentration, elongating minority carrier lifetime, and so on). Thus, sodium doping becomes an effective modification means for Cu_2ZnSnS_4 on the flexible substrate. However, there are some examples available in the literature that discuss the underlying physical mechanism. In the present work, the crystal structure, electronic structure, and optical properties of sodium occupying different lattice sites or interstitial sites of kesterite Cu_2ZnSnS_4 were systematically calculated by density functional theory within the GGA+U method. Na impurity favors occupation of the interstitial sites. If Na impurity occupies the cation lattice sites, the band gap of Cu_2ZnSnS_4 will be broadened, which is opposite to the situation of an Na impurity occupying the interstitial sites. The doping effects of Na in Cu_2ZnSnS_4 are mainly exhibited by the following aspects: energy band shifting, energy band broadening or narrowing, and effective mass of holes on the top of valence band reduction. The calculated results in the present work not only confirm experimental observationa in published articles but also provide an in-depth understanding of them. Thus, the findings could help to promote novel, high-efficiency Cu_2ZnSnS_4-based thin-film solar cells.

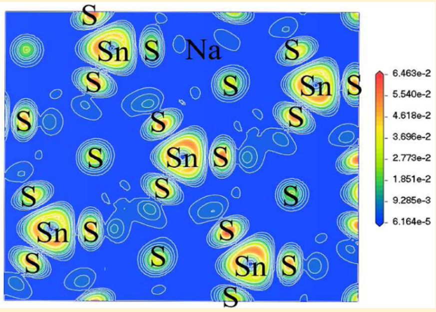

1. INTRODUCTION

As a multifunctional quaternary compound semiconductor, Cu_2ZnSnS_4 (CZTS) in recent years has attracted more and more attention, such as applications in solar cells,[1,2] photocatalysis,[3] and thermoelectricity.[4] Especially in the field of solar cell applications, it is a very promising material for use as a low-cost absorber alternative to $Cu(In,Ga)Se_2$ (CIGS), because it is composed of only abundant, nontoxic, and economical elements.[5−9] In addition, CZTS has a direct band gap energy of 1.0−1.5 eV, a large absorption coefficient of over 10^4 cm^{-1}, and excellent photoelectric properties similar to those of CIGS, which is regarded as one of the best absorber materials for sustainable and highly efficient thin-film solar cells. In 1967, Nitsche et al. successfully prepared CZTS single crystals using an iodine vapor transport method,[10] in 1988, Ito et al. prepared a CZTS thin film by an electron beam vapor deposition method,[11] and in 1997, Katagiri et al. succeeded in assembling the first CZTS-based thin-film solar cell with a photoelectric conversion efficiency of 0.66%.[12] However, the best photoelectric conversion efficiency of a CZTS-based thin film solar cell to date is 8.4%,[13] which is still much lower than the high conversion efficiency of 20.4% obtained for CIGS-based thin-film solar cells[14] and the theoretical limit of conversion efficiency (32.2%) for CZTS-based thin-film solar cells by Shockley−Queisser photo balance calculations.[15] Thus, it is necessary to obtain a more detailed understanding of the microstructure and fundamental properties of CZTS.

In order to improve the photoelectric conversion efficiency of CZTS-based solar cells, researchers have attempted various modification means. The common method is to synthesize a $Cu_2ZnSn(S,Se)_4$ (CZTSSe) solid solution. In 2013, Mitzi et al. prepared a CZTSSe-based thin film solar cell through a nonvacuum hydrazine solution method and gained a high photoelectric conversion efficiency of 12.6%, which is close to the applied standard.[16] In addition, the construction of a solar cell device has also attracted attention: for example, grain boundary, interface, antireflection layer, buffer layer, and so on. It is very noteworthy that the best CZTS-based thin-film solar cells used soda−lime glass (SLG) substrates in combination with high growth temperatures of around 550 °C. In the high-temperature processing, sodium (Na) impurities are inevitably diffused into the absorber layer and the interfaces between different layers. In CIGS-based thin-film solar cells, the effects of Na include an enhancement of preferred orientation and grain size, a decrease in resistivity, and an improved open-circuit voltage and cell performance.[17] The similar effects of Na were observed in CZTS-based thin-film solar cells.[18,19] Recently, Nagaoka et al. have studied the effect of Na incorporation in CZTS single crystals and influence on the electrical properties using the temperature dependence of Hall effect measurements and revealed that Na is an important dopant in CZTS single crystals to control the electrical

Received: June 9, 2014
Published: August 18, 2014

properties and provided a useful understanding in improving the efficiency of CZTS solar cells.[20] To sum up, the doping effects of Na could improve the photovoltaic performance in the following aspects: influencing crystallinity, affecting grain growth, increasing hole density, shifting the acceptor level closer to the conduction band, increasing carrier concentration, elongating minority carrier lifetime, and so on.[21−26] On the basis of the doping effects of Na, researchers proposed a novel Na-containing precursor solution to prepare suitable CZTS thin films directly on flexible substrates other than rigid substrates of soda−lime glass,[24,27] which is very important in expanding the applications of CZTS. However, only a few studies are available that give a fundamental understanding of the doping effect of Na on CZTS.

To better understand the in-depth physical properties of the doping effect of Na on CZTS, we systematically investigated the crystal structure, electronic structure, and optical properties of Na-doped kesterite CZTS in the present work, in which Na occupies the cation sites and the interstitial sites, using first-principles calculations based on density functional theory (DFT). With use of the calculated results, the relationship between photovoltaic performance and Na impurity will be discussed, and a possible explanation for previous experimental observations will be provided. The findings of the present work should help to clarify some previous conclusions in the published articles and promote the development of novel, highly efficient CZTS-based thin-film solar cells.

2. COMPUTATIONAL METHODS

In the present work, all the first-principles calculations were implemented in the framework of density functional theory within the generalized gradient approximation (GGA) using the PBE exchange correlation potential and utilizing the plane-wave total energy pseudopotential method as implemented in the CASTEP code.[28−30] The ion−electron interaction is modeled by ultrasoft pseudopotential in the Vanderbilt form,[31] which has yielded satisfactory results in recent studies using the aforementioned methods. The valence atomic configurations are $2s^22p^63s^1$ for Na, $3d^{10}4s^1$ for Cu, $3d^{10}4s^2$ for Zn, $5s^25p^2$ for Sn, and $3s^23p^4$ for S. The energy cutoff for the plane wave basis set was 440 eV. In order to obtain an accurate electronic structure, the method of GGA+U was adopted to overcome the well-known shortcomings of GGA.[32] The Hubbard model is one of the most successful models in describing the correlated electrons in solids. To construct an appropriate functional, the GGA+U approach subdivides charge density into two subsystems: delocalized and localized. The former remains described by its charge density, while for the latter a site diagonal charge density matrix is introduced. In the present work, the U value of a metallic element d orbital was set as follows: $U_{\text{eff}} = U - J = 5.00$ eV, which is obtained by comparing the calculated and measured band gaps of kesterite CZTS. The Monkhorst−Pack scheme k-point grid sampling was set as $2 \times 2 \times 2$ for the irreducible Brillouin zone. A $80 \times 80 \times 75$ mesh was used for fast Fourier transformation. The Broyden−Fletcher−Goldfarb−Shanno (BFGS) scheme was chosen as the minimization algorithm.[33] Its convergence criteria were set as follows: the forces on the atoms were less than 0.01 eV/Å, the stresses on the atoms were less than 0.02 GPa, the atomic displacement was less than 5×10^{-4} Å, and the energy change per atom was less than 5×10^{-6} eV. On the basis of the optimized crystal structure, the electronic structure and optical properties were then calculated. Using the above computational method, we obtained the lattice constants of pure kesterite CZTS as follows: $a = b = 5.4709$ Å, $c = 10.9387$ Å, which is very close to the experimental measurement:[6,34] $a = b = 5.43$ Å and $c = 10.89$ Å, suggesting that the computational method in the present work was reasonable.

In the present work, $2 \times 2 \times 1$ supercells were used for constructing the Na-doped kesterite CZTS models. To set the substitutional doping models, one copper atom, one zinc atom, or one tin atom in the supercell was replaced by one sodium atom, which will be notated by Na@Cu, Na@Zn, and Na@Sn in the following text. In addition, to set the interstitial doping models, one sodium atom occupies the vacancy of the tetrahedron, which will be notated by Na@Vac in the following text. For the crystal structure of kesterite CZTS, there are two copper lattice sites, one zinc lattice site, one tin lattice site, and three kinds of vacancies between the tetrahedrons (CuS_4, ZnS_4, and SnS_4). Thus, we considered four substitutional models and three interstitial models.

3. RESULTS AND DISCUSSION

3.1. Crystal Structure. First, the lattice parameters of Na-doped CZTS models were analyzed, and the results are presented in Table 1. When Na impurity is introduced into the host lattice, lattice distortion usually occurs, due to the differences of ion radius and valence electron configuration. However, in the present work, we found that the lattice distortions are very slight for the four kinds of Na-doped CZTS models. Therefore, even with implantation of an Na impurity, kesterite CZTS still could maintain its exceptional photovoltaic performance.[24] While Na@Sn doping induces shortening of the lattice constant c, Na doping elongates the lattice constants. In addition, Na doping causes the crystal volume to expand for all models, which is quite consistent with experimental observations.[20,26,27] In these models, the crystal expansion of the Na@Sn model is the smallest, while that of the Na@Vac model is the largest.

Table 1. Variation of Lattice Constants of Kesterite CZTS by Na Impurity Doping on Different Lattice Positions and the Corresponding Impurity Formation Energy

	Δa/Å	Δc/Å	ΔV/Å^3	E_f/eV
Na@Cu	0.0461	0.0138	5.965	3.4429
Na@Zn	0.0327	0.0237	4.647	2.0916
Na@Sn	0.0246	−0.0295	2.065	4.6270
Na@Vac	0.0634	0.0920	10.437	0.5506

Because there are two different lattice positions for sodium replacing copper and three different vacancies for sodium interstitial doping, we therefore first put the point defects on different positions and compared the corresponding impurity formation energies (E_f) to determine the stable structure for each Na-doped model. This is a widely accepted approach to compare the relative degree of difficulty for different defects incorporated into the host lattice. In the present work, the formula of impurity formation energy is referred to the formalism defined by Van de Walle et al.[35] In the case of Na@Cu models, when Na occupies the Cu_1 sites, in which Cu atoms are on the same plane with Sn atoms along the [001] direction, the impurity formation energy is smaller by ~0.0478 eV than that of Na occupying the Cu_2 sites, in which Cu atoms are on the same plane with Zn atoms along the [001] direction. In addition, the impurity formation energy of Na occupying the interstitial site near the CuS_4 tetrahedron is the smallest (smaller by ~0.2 eV). The calculated smallest impurity formation energies are also presented in Table 1. On comparison of these data, it is could be found that the impurity formation energy of the Na@Vac model is obviously smaller than that of other models. Therefore, Na occupying the interstitial sites is a relatively stable doping fashion. Meanwhile, this calculated result means that sodium ions could easily

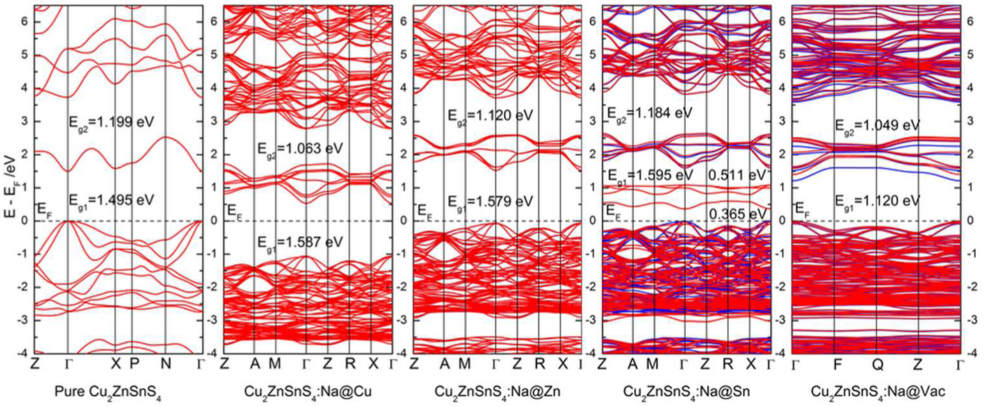

Figure 1. Calculated band structures of kesterite CZTS and Na-doped CZTS and the corresponding distance between energy bands. The blue lines represent spin-up states, while the red lines represent spin-down states.

diffuse the interstitial channels in the host of kesterite CZTS. Thus, in the experimental high-temperature processing, sodium ions could diffuse through the CZTS absorber layer to the interface between the absorber layer and the buffer layer, resulting in finally influencing the device's microstructure and the photovoltaic performance of CZTS-based thin-film solar cells.

3.2. Electronic Structure. The calculated band structures of all models are plotted and compared in Figure 1. As shown in Figure 1, we found that pure kesterite CZTS is a direct band gap semiconductor, with a band gap of 1.495 eV between the maximum of the valence band (VBM) and the minimum of the conduction band (CBM), which very close to the experimental measurements (E_g = 1.49 eV).[6,34] Furthermore, the conduction band of pure kesterite CZTS is divided into two distinct parts: the first part is an isolated band away from the main conduction band with another band gap of 1.199 eV. This phenomenon was observed in previous theoretical works in published studies.[5,36,37] In order to distinguish these bands, we defined the lowest conduction band as CB_1, which has a band gap of E_{g1} with the valence band, and the lower conduction band as CB_2, which has a band gap of E_{g2} with CB_1. For pure kesterite CZTS, the spin-up states coincide with the spin-down states, owing to the completely paired valence electrons. When a sodium impurity is implemented into CZTS, the first effect is symmetry decrease: the symmetry group of pure kesterite CZTS is $I\overline{4}$, while in the cases of Na-substituted doping models the symmetry group is $P\overline{4}$ and in the case of Na interstitial doping models the symmetry group is $P1$. Thus, in the band structure, the degenerate energy levels are split: namely, the degeneracy is lifted, which is especially obvious in the case of the Na@Vac model. In the cases of Na@Cu and Na@Zn models, the spin-up states still coincide with the spin-down states, while in the cases of Na@Sn and Na@Vac models, the spin-up states do not coincide with the spin-down states. Therefore, there are no energy levels induced by Na impurity in the band gap of Na@Cu and Na@Zn models. However, there are spin-down energy levels (with a bandwidth of 0.72 eV) induced by Na impurity in the first band gap of the Na@Sn model, which are deep impurity energy levels, and there is a spin-up energy level at the bottom of first conduction band of the Na@Vac model, which is a shallow acceptor energy level. Another noticeable change is the shifting of energy bands in the Na@Cu model. As shown in Figure 1, the impurity energy levels of the Na@Sn model form an isolated energy band that is separated from VBM (or CBM) by 0.365 eV (or 0.511 eV), while the impurity energy level of the Na@Vac model is overlapping with the bottom of the CB. Because the position of the Fermi energy level (E_F) is fixed at 0 eV, the shifting of energy bands means the relative movement of E_F. Thus, E_F shifts relatively upward in the Na@Cu model, while it is maintained at the top of the valence band in the other three doped models. The changes in band gap and bandwidth caused by symmetry variance are given in Table 2.

Table 2. Parameters of Band Structure of Kesterite CZTS and the Na-Doped CZTS, Including Band Gap and Band Width (in eV)

	E_{g1}	E_{g2}	W_{VB}	W_{CB1}	W_{CB2}	W_{Im}
pure	1.495	1.199	2.856	1.035	2.372	
Na@Cu	1.587	1.063	2.671	1.191	2.304	
Na@Zn	1.579	1.120	2.868	1.069	2.338	
Na@Sn	1.595	1.184	3.033	1.044	2.234	0.720
Na@Vac	1.120	1.049	2.949	1.327	2.362	

These changes can be briefly described as follows: the first band gap (E_{g1}) is increased except in the case of the Na@Vac model; the second band gap (E_{g2}) is decreased except in the case of the Na@Zn model; the width of the valence band (W_{VB}) is increased, except in the case of the Na@Cu model; the width of the first conduction band (W_{CB1}) is increased for all models, while the width of the second conduction band (W_{CB2}) is decreased for all models. However, these changes are not noticeable except in the case of the Na@Vac model. In the case of the Na@Vac model, both band gaps are obviously decreased, owing to the first conduction band broadening.

In order to further explain the doping effect, we fitted the energy–momentum dependence of the energy states at VBM and CBM and got the minimum of effective mass for electrons or holes, which are given in Table 3. The minimum of effective mass of photogenerated electrons on the bottom of conduction band is ~$0.22m_0$, which is obviously smaller than that of the typical oxide semiconductors (such as $m_e^* \approx 1m_0$ of anatase TiO_2[38] and $m_e^* \approx 3-20m_0$ of rutile TiO_2[39,40]). In addition, the minimum effective mass of photogenerated holes at the top of the valence band is ~$0.66m_0$, which is also obviously smaller than that of oxide semiconductors (such as $m_h^* \approx 16m_0$ of In_2O_3[41]). In the field of photoelectric applications, the effective mass of photogenerated carriers is lighter, implying that the carriers have more probability to reach the interface of devices

Table 3. Effective Mass of Holes at the Valence Band Maximum or Electrons at the Conduction Band Minimum along the Different Directions, on the Basis of the Calculated Band Structure of Kesterite CZTS and Na-Doped CZTS

	m_h^*/m_0			m_e^*/m_0		
pure	$\Gamma \rightarrow Z$ $([\bar{1}\bar{1}1])$: 0.664	$\Gamma \rightarrow X([001])$: 3.854	$\Gamma \rightarrow N([0\bar{1}0])$: 0.851	$\Gamma \rightarrow Z([\bar{1}\bar{1}1])$: 0.256	$\Gamma \rightarrow X([001])$: 0.226	$\Gamma \rightarrow N([0\bar{1}0])$: 0.221
Na@Cu	$\Gamma \rightarrow M([\bar{1}\bar{1}0])$: 0.876	$\Gamma \rightarrow Z([001])$: 0.241	$\Gamma \rightarrow X([0\bar{1}0])$: 0.869	$\Gamma \rightarrow M([\bar{1}\bar{1}0])$: 0.276	$\Gamma \rightarrow Z([001])$: 0.310	$\Gamma \rightarrow X([0\bar{1}0])$: 0.263
Na@Zn	$\Gamma \rightarrow M([\bar{1}\bar{1}0])$: 0.879	$\Gamma \rightarrow Z([001])$: 0.245	$\Gamma \rightarrow X([0\bar{1}0])$: 0.853	$\Gamma \rightarrow M([\bar{1}\bar{1}0])$: 0.255	$\Gamma \rightarrow Z([001])$: 0.275	$\Gamma \rightarrow X([0\bar{1}0])$: 0.243
Na@Sn	$\Gamma \rightarrow M([\bar{1}\bar{1}0])$: 0.891	$\Gamma \rightarrow Z([001])$: 0.249	$\Gamma \rightarrow X([0\bar{1}0])$: 0.911	$\Gamma \rightarrow M([\bar{1}\bar{1}0])$: 0.268	$\Gamma \rightarrow Z([001])$: 0.325	$\Gamma \rightarrow X([0\bar{1}0])$: 0.256
Na@Vac	$\Gamma \rightarrow F([010])$: 0.527	$\Gamma \rightarrow Z([00\bar{1}])$: 0.406		$\Gamma \rightarrow F([010])$: 0.283	$\Gamma \rightarrow Z([00\bar{1}])$: 0.354	

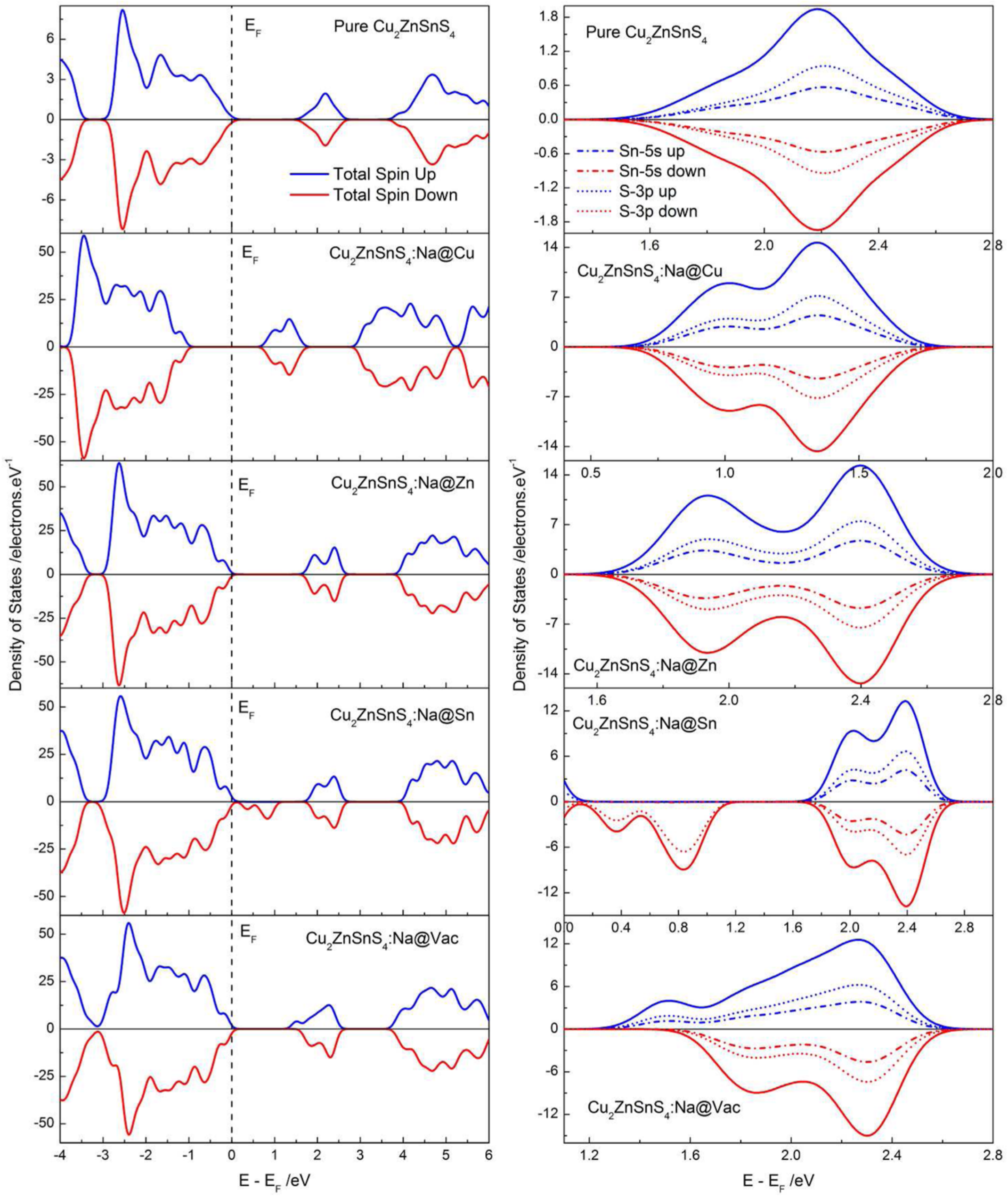

Figure 2. Calculated total density of states of kesterite CZTS and Na-doped CZTS. The corresponding local and partial densities of states of the first conduction band or impurity energy band are also presented.

within their lifetime, thus improving the photoelectric performance. Therefore, the light effective mass of photogenerated carriers in kesterite CZTS should favor the separation of electron−hole pairs and improvement of photovoltaic properties. We found that Na doping could reduce the effective mass of holes at the top of VB; in particular, Na impurity occupies the cation lattice sites. This calculated result means that Na impurity occupation of the cation lattice sites could increase the diffusion length of photoexcited holes, so that more holes could reach the interface of solar cell devices during their limited

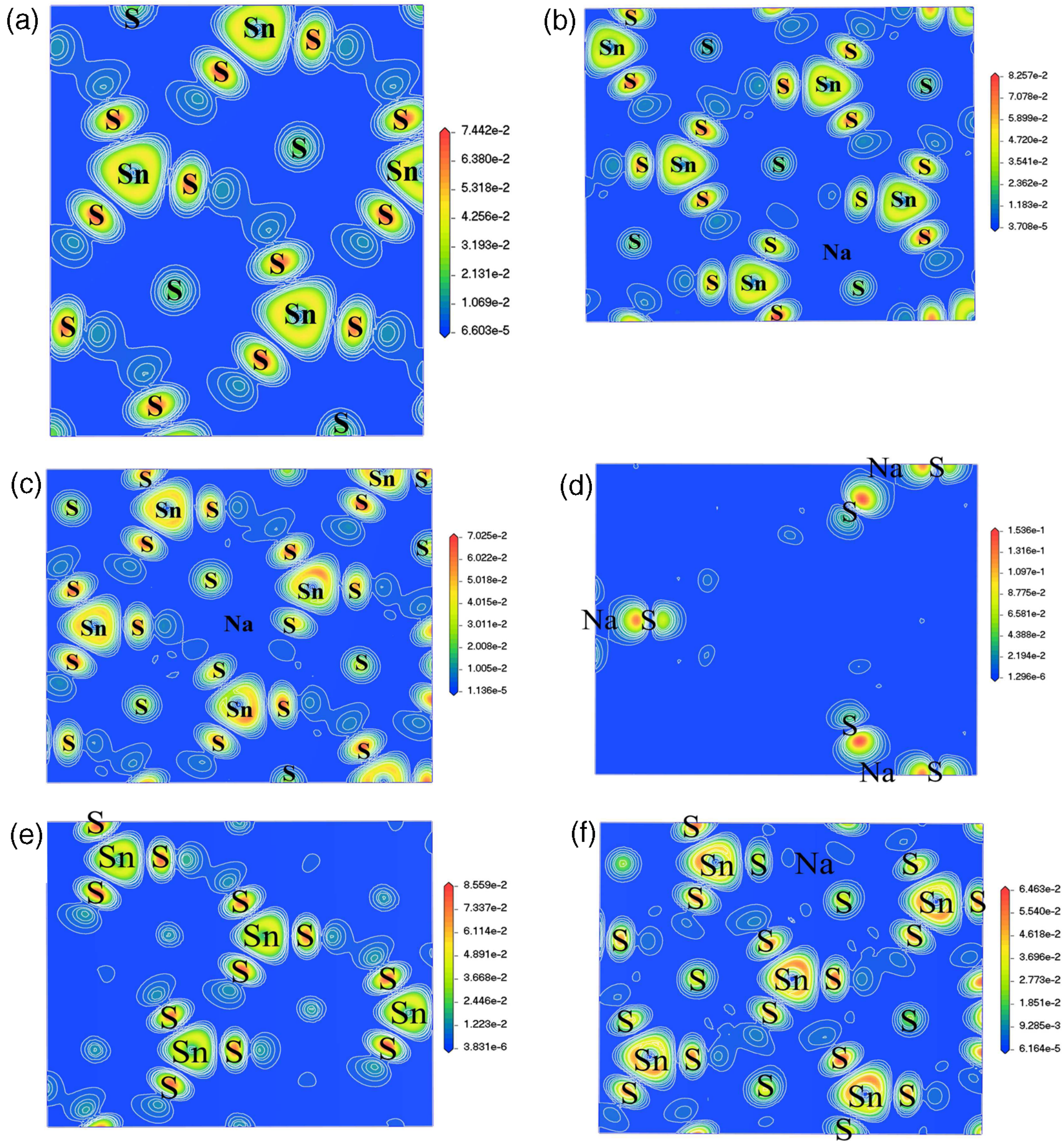

Figure 3. Projected contour maps of electronic wave functions of the first conduction band along the (112) plane: (a) pure Cu_2ZnSnS_4; (b) Cu_2ZnSnS_4:Na@Cu; (c) Cu_2ZnSnS_4:Na@Zn; (d) Cu_2ZnSnS_4:Na@Sn (the impurity energy band); (e) Cu_2ZnSnS_4:Na@Sn; (f) Cu_2ZnSnS_4:Na@Vac.

lifetime. Thus, the carrier concentration will be increased, the hole mobility will be enhanced, and minority carrier lifetime will be elongated for the CZTS-based thin-film solar cell devices, which is in agreement with experimental measurements.[20,23,24] However, at the same time, the effective mass of electrons at the bottom of the valence band is slightly increased by Na doping.

To clearly analyze the chemical bonding features, the density of states (DOS) and projected contour maps of electronic wave functions of the first conduction band along the (112) plane are respectively illustrated and compared in Figures 2 and 3. In the case of pure kesterite CZTS, the calculated DOS is very consistent with previously reported results by other computational methods.[5,42] After Na doping, the main features of the valence band and the second band are not obviously changed. As shown in Figures 2 and 3, the first conduction band is mainly composed of the hybridization between S 3p states and Sn 5s states. The doping effects are mainly exhibited by the variation of the first conduction band, combined with the top of the valence band and the bottom of the second conduction band. In the case of pure kesterite CZTS, the DOS peak corresponding to the first conduction band is very compact, while in the cases of Na-doped CZTS models, this peak is divided into two distinct peaks. This phenomenon is especially obvious in the case of the Na@Zn model. As mentioned above, the spin-up states are not coincident with the spin-down states in the cases of Na@Sn and Na@Vac models, which are also clearly exhibited in the DOS figures. As shown in Figure 3d, in the case of the Na@Sn model, the impurity energy band is dominantly composed by the S 3p states near the Na impurities. In the case of the Na@Vac model, the separated spin-up states become the shallow acceptor states, while the two distinct spin-down peaks are similar to those of other Na doping models. In combination with the results discussed above regarding the electronic structure, the doping effects of Na are mainly exhibited by the following aspects: energy band shifting and energy band broadening and narrowing. However, the electronic states of Na do not take part in the variation of electronic states near the band gap, implying that the doping effects are indirectly presented by the interaction of Na impurity with its neighboring atoms in the host of CZTS.

3.3. Optical Properties. The calculated absorption spectra of pure kesterite CZTS and Na-doped CZTS by the polycrystalline model are displayed in Figure 4. The spectrum of pure kesterite CZTS is fully consistent with the experimental measurements.[43] On the basis of the electronic structure calculations, the band gap between the valence band and the second conduction band could be defined as follows: $E_{g3} = E_{g1} + E_{g2} + W_{CB1}$, as the discussion in our previous works.[44] Thus, when electrons on the top of VB absorb the incident photo energy, there are three kinds of electron transitions: VB → CB_1, CB_1 → CB_2, and VB → CB_2, whose transition energies correspond to E_{g1}, E_{g2}, and E_{g3}, respectively. In the absorption spectrum of pure kesterite CZTS, we could identify the absorption peak centered at 640 nm as arising from the electron transition between the top of VB to the bottom of CB_1, the absorption peak centered at 500 nm as arising from the electron transition between the top of VB to the top of CB_1, and absorption peaks above 400 nm as arising from the electron transition from the top of VB to the bottom of CB_2. Because CB_1 is an unoccupied band above the Fermi energy level, in the current first-principles calculations only the electron transition between occupied states and unoccupied states is considered. Thus, the absorption peaks corresponding to the electron transitions CB_1 → CB_2 and VB → CB_1 → CB_2 were not calculated. For Na-doped CZTS, the fundamental absorption edge is blue-shifted when Na occupies the cation lattice sites, while the fundamental absorption edge is red-shifted when Na occupies the interstitial sites. In experiments, the difference in absorption edges caused by different Na doping is also observed.[26,27] Importantly, Na doping enhances the absorption of CZTS in the visible-light region for all models. Due to the existence of impurity energy levels in the Na@Sn model, CZTS could absorb sunlight whose wavelength is larger than 800 nm, which is a very helpful response of a CZTS-based thin-film solar cell to a lower-energy photon. These optical phenomena are rooted in the variation of the first band gap and the composition of an energy band near the band gap.

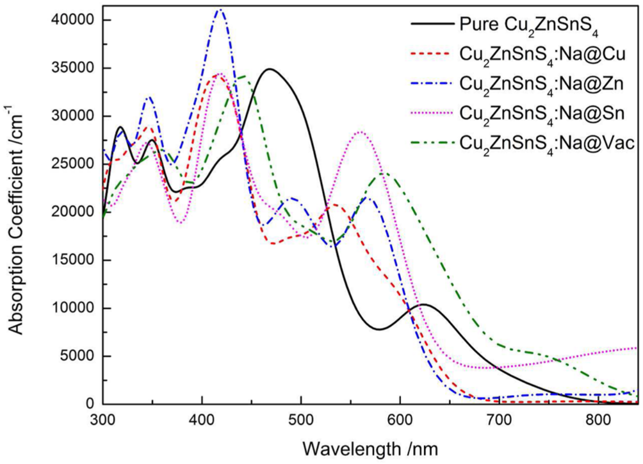

Figure 4. Calculated absorption spectrum of kesterite CZTS and Na-doped CZTS.

There have been only a few studies that report the optical properties of Na-doped CZTS. Li et al. provided the optical band gap of different Na-doped CZTS samples with various Na contents and observed that a blue shift of the absorption edge along with an increase in Na content.[27] However, these experimental phenomena are also caused by other effects, such as other defects, crystallization, etc. In the present work, the direct evidence of optical property variation caused by Na-doped CZTS at different lattice sites is provided, which is very helpful in understanding the related experimental phenomena. On the basis of these calculated results, the different variations of optical absorption in the different wavelength ranges of Na-doped CZTS are worth considering, in addition to different Na doping concentrations or doping lattice sites. As shown in Figure 4, the absorption bands are blue-shifted fpr all Na-doped CZTS samples, in comparison with that of pure CZTS, except for the variation in fundamental absorption edge. The absorption bands centered at 630 and 460 nm are respectively blue-shifted to 560 and 420 nm. Moreover, the blue shift of the Na@Cu model is the most obvious, while that of Na@Vac is the least obvious. In other words, the optical absorption of CZTS will be enhanced by Na doping when the incident photon wavelength is smaller than 440 nm or larger than 530 nm, while its optical properties will be reduced by Na doping when the incident photon wavelength is in the range of 440−530 nm.

4. CONCLUSIONS

In order to systematically investigate the doping effect of sodium in kesterite CZTS, the crystal structure, electronic structure, and optical properties of Na occupying different lattice sites or interstitial sites of kesterite CZTS were calculated by density functional theory within the GGA+U method. In the crystal structure, Na doping causes very gentle lattice distortion and induces crystal expansion in all Na-doped CZTS models. When Na occupies the cation lattice sites, the first band gap of CZTS is broadened, while it is narrowed when Na occupies the interstitial sites. In the case of Na occupation of the Sn lattice sites, there is an impurity energy level in the middle of the first band gap, which predominantly consists of the S 3p states near the Na impurity. In the case of Na occupation of the interstitial sites, there is a shallow acceptor level at the bottom of the first conduction band, owing to the lifting of degeneracy. The doping effects of Na are mainly exhibited by the following aspects: energy band shifting and energy band broadening and narrowing. However, the electronic states of Na do not take part in the variation of electronic states near the band gap, implying that the doping effects are indirectly presented by the interaction of Na impurity with its neighboring atoms in the host of CZTS. Importantly, Na doping could reduce the effective mass of holes on the top of the valence band. Thus, the carrier concentration will be increased, the hole mobility will be enhanced, and minority carrier lifetime will be elongated for the CZTS-based thin-film solar cell devices. With regard to optical properties, the fundamental absorption edge of CZTS is blue-shifted when Na occupies the cation lattice sites, while the fundamental absorption edge is red-shifted when Na occupies the interstitial sites. In addition, the optical absorption of CZTS will be enhanced in most wavelength ranges, except for the narrow range of 440−530 nm.

■ AUTHOR INFORMATION

Corresponding Author

*Z.-Y.Z.: e-mail, zzy@kmust.edu.cn; tel, +86-871-65109952; fax, +86-871-65107922.

Notes

The authors declare no competing financial interest.

■ ACKNOWLEDGMENTS

The authors acknowledge financial support from the National Natural Science Foundation of China (Grant No. 21263006), the Science Research Foundation of Educational Commission of Yunnan Province of China (Grant No. 2012Y542), and the Introduced Talents Foundation of the Kunming University of Science and Technology. The present work was supported by the analysis and testing foundation of the Kunming University of Science and Technology (Grant No. 20130196).

■ REFERENCES

(1) Fella, C. M.; Romanyuk, Y. E.; Tiwari, A. N. *Sol. Energy Mater. Sol. Cells* **2013**, *119*, 276−277.

(2) Chen, S.; Walsh, A.; Gong, X.-G.; Wei, S.-H. *Adv. Mater.* **2013**, *25*, 1522−1539.

(3) Wang, P.; Minegishi, T.; Ma, G.; Takanabe, K.; Satou, Y.; Maekawa, S.; Kobori, Y.; Kubota, J.; Domen, K. *J. Am. Chem. Soc.* **2012**, *134*, 2469−2472.

(4) Yang, H.; Jauregui, L. A.; Zhang, G.; Chen, Y. P.; Wu, Y. *Nano Lett.* **2012**, *12*, 540−545.

(5) Paier, J.; Asahi, R.; Nagoya, A.; Kresse, G. *Phys. Rev. B* **2009**, *79*, 115126.

(6) Scragg, J. J.; Dale, P. J.; Peter, L. M.; Zoppi, G.; Forbes, I. *Phys. Status Solidi B* **2008**, *245*, 1772−1778.

(7) Katagiri, H.; Jimbo, K.; Maw, W. S.; Oishi, K.; Yamazaki, M.; Araki, H.; Takeuchi, A. *Thin Solid Films* **2009**, *517*, 2455−2460.

(8) Guo, Q.; Ford, G. M.; Yang, W.-C.; Walker, B. C.; Stach, E. A.; Hillhouse, H. W.; Agrawal, R. *J. Am. Chem. Soc.* **2010**, *132*, 17384−17386.

(9) Steinhagen, C.; Panthani, M. G.; Akhavan, V.; Goodfellow, B.; Koo, B.; Korgel, B. A. *J. Am. Chem. Soc.* **2009**, *131*, 12554−12555.

(10) Nitsche, R.; Sargent, D. F.; Wild, P. *J. Cryst. Growth* **1967**, *1*, 52−53.

(11) Ito, K.; Nakazawa, T. *Jpn. J. Appl. Phys.* **1988**, *27*, 2094.

(12) Katagiri, H.; Sasaguchi, N.; Hando, S.; Hoshino, S.; Ohashi, J.; Yokota, T. *Sol. Energy Mater. Sol. Cells* **1997**, *49*, 407−414.

(13) Shin, B.; Gunawan, O.; Zhu, Y.; Bojarczuk, N. A.; Chey, S. J.; Guha, S. *Prog. Photovoltaics* **2013**, *21*, 72−76.

(14) Powalla, M.; Jackson, P.; Witte, W.; Hariskos, D.; Paetel, S.; Tschamber, C.; Wischmann, W. *Sol. Energy Mater. Sol. Cells* **2013**, *119*, 51−58.

(15) Yoo, H.; Kim, J. *Sol. Energy Mater. Sol. Cells* **2011**, *95*, 239−244.

(16) Wang, W.; Winkler, M. T.; Gunawan, O.; Gokmen, T.; Todorov, T. K.; Zhu, Y.; Mitzi, D. B. *Adv. Eng. Mater.* **2014**, xx DOI: 10.1002/aenm.201301465.

(17) Nakada, T.; Iga, D.; Ohbo, H.; Kunioka, A. *Jpn. J. Appl. Phys.* **1997**, *36*, 732.

(18) Yang, K.-J.; Sim, J.-H.; Jeon, B.; Son, D.-H.; Kim, D.-H.; Sung, S.-J.; Hwang, D.-K.; Song, S.; Khadka, D. B.; Kim, J.; Kang, J.-K. *Prog. Photovolt.: Res. Appl.* **2014**, DOI: 10.1002/pip.2500.

(19) Prabhakar, T.; Jampana, N. *Sol. Energy Mater. Sol. Cells* **2011**, *95*, 1001−1004.

(20) Nagaoka, A.; Miyake, H.; Taniyama, T.; Kakimoto, K.; Nose, Y.; Scarpulla, M. A.; Yoshino, K. *Appl. Phys. Lett.* **2014**, *104*, 152101.

(21) Repins, I.; Beall, C.; Vora, N.; DeHart, C.; Kuciauskas, D.; Dippo, P.; To, B.; Mann, J.; Hsu, W.-C.; Goodrich, A.; Noufi, R. *Sol. Energy Mater. Sol. Cells* **2012**, *101*, 154−159.

(22) Hlaing Oo, W. M.; Johnson, J. L.; Bhatia, A.; Lund, E. A.; Nowell, M. M.; Scarpulla, M. A. *J. Electron. Mater.* **2011**, *40*, 2214−2221.

(23) Li, J. V.; Kuciauskas, D.; Young, M. R.; Repins, I. L. *Appl. Phys. Lett.* **2013**, *102*, 163905.

(24) Zhou, H.; Song, T.-B.; Hsu, W.-C.; Luo, S.; Ye, S.; Duan, H.-S.; Hsu, C.-J.; Yang, W.; Yang, Y. *J. Am. Chem. Soc.* **2013**, *135*, 15998−16001.

(25) Prabhakar, T.; Nagaraju, J. In Alkali assisted enhancement of CZTS absorber layer characteristics. Photovoltaic Specialists Conference (PVSC), 2011 37th IEEE, June 19−24, 2011; IEEE: Seattle, WA, pp 001357−001361.

(26) Sutter-Fella, C. M.; Stückelberger, J. A.; Hagendorfer, H.; La Mattina, F.; Kranz, L.; Nishiwaki, S.; Uhl, A. R.; Romanyuk, Y. E.; Tiwari, A. N. *Chem. Mater.* **2014**, *26*, 1420−1425.

(27) Li, Y.; Han, Q.; Kim, T.; Shi, W. *J. Sol-Gel Sci. Technol.* **2014**, *69*, 260−265.

(28) Kohn, W.; Becke, A. D.; Parr, R. G. *J. Phys. Chem.* **1996**, *100*, 12974−12980.

(29) Perdew, J. P.; Burke, K.; Ernzerhof, M. *Phys. Rev. Lett.* **1996**, *77*, 3865.

(30) Perdew, J. P.; Chevary, J.; Vosko, S.; Jackson, K. A.; Pederson, M. R.; Singh, D.; Fiolhais, C. *Phys. Rev. B* **1992**, *46*, 6671.

(31) Bernardini, F.; Fiorentini, V.; Vanderbilt, D. *Phys. Rev. B* **1997**, *56*, R10024.

(32) Anisimov, V. I.; Zaanen, J.; Andersen, O. K. *Phys. Rev. B* **1991**, *44*, 943.

(33) Pfrommer, B. G.; Câté, M.; Louie, S. G.; Cohen, M. L. *J. Comput. Phys.* **1997**, *131*, 233−240.

(34) Sekiguchi, K.; Tanaka, K.; Moriya, K.; Uchiki, H. *Phys. Status Solidi C* **2006**, *3*, 2618−2621.

(35) Van de Walle, C. G.; Neugebauer, J. *J. Appl. Phys.* **2004**, *95*, 3851−3879.

(36) Botti, S.; Kammerlander, D.; Marques, M. A. L. *Appl. Phys. Lett.* **2011**, *98*, 241915.

(37) Zhang, Y.; Yuan, X.; Sun, X.; Shih, B.-C.; Zhang, P.; Zhang, W. *Phys. Rev. B* **2011**, *84*, 075127.

(38) Tang, H.; Prasad, K.; Sanjines, R.; Schmid, P. E.; Levy, F. *J. Appl. Phys.* **1994**, *75*, 2042−2047.

(39) Pascual, J.; Camassel, J.; Mathieu, H. *Phys. Rev. Lett.* **1977**, *39*, 1490.

(40) Frederikse, H. P. R. *J. Appl. Phys.* **1961**, *32*, 2211−2215.

(41) Walsh, A.; Da Silva, J. L. F.; Wei, S.-H. *Phys. Rev. B* **2008**, *78*, 075211.

(42) Chen, S.; Gong, X. G.; Walsh, A.; Wei, S.-H. *Appl. Phys. Lett.* **2009**, *94*, 041903−3.

(43) Mali, S. S.; Patil, P. S.; Hong, C. K. *ACS Appl. Mater. Interfaces* **2014**, *6*, 1688−1696.

(44) Zhao, Z.; Ma, C.; Cao, Y.; Yi, J.; He, X.; Qiu, J. *Phys. Lett. A* **2013**, *377*, 417−422.